Proceedings of the 1998 IEEE
International Conference on Control Applications
Trieste, Italy 1-4 September 1998

TP05

$\mathcal{H}_\infty$-BASED ROBUST TORQUE CONTROL OF HARMONIC DRIVE SYSTEMS UNDER FREE- AND CONSTRAINED-MOTION APPLICATIONS

H.D. Taghirad
K. N. Toosi U. of Technology,
Dept. of Elec. Eng.,
P.O. Box 16315 - 1355,
E-mail: taghirad@eetd.kntu.ac.ir

P.R. Bélanger
Center for Intelligent Machines,
McGill University,
Montréal, PQ, H3A 2A7
E-mail: pbelanger@fgsr.mcgill.ca

ABSTRACT

In this paper the torque control of a harmonic drive system for constrained-motion and free-motion applications is examined in detail. A nominal model for the system is obtained in each case from experimental frequency responses of the system, and the deviation of the system from the model is encapsulated by a multiplicative uncertainty. Robust torque controllers are designed using these information in an $\mathcal{H}_\infty$ -framework, and implemented on two different setups. From time and frequency domain experiments, it is shown that the closed-loop system retains robust stability, while improving the tracking performance exceptionally well.

I. INTRODUCTION

Developed in 1955 primarily for aerospace applications, harmonic drives are high-ratio and compact torque transmission systems. The harmonic drive exhibits performance features both superior and inferior to those of conventional gear transmissions. Its performance advantages include high-torque capacity, concentric geometry, lightweight and compact design, zero backlash, high efficiency, and back drivability. Harmonic drive systems suffer however, from high flexibility, resonance vibration, friction and structural damping nonlinearities.

In numerous robotic control techniques the actuator torque is taken to variable being manipulated in practice, however, is not torque but armature current in a DC motor, for instance. For harmonic drive systems the relation between output torque and input current possesses nonlinear dynamics, due to the flexibility, Coulomb friction and structural damping of the harmonic drive [6]. Therefore, it is desired to improve this input/output relation by torque feedback, and to convert the system to a near-ideal torque source with a flat frequency response over a wide bandwidth. There are two types of torque-control applications for a robot manipulator using harmonic drives in its joints. First the applications where the robot is in contact with a stiff environment, and high torques at very low velocities are required at each joint. Simulation of this application at each joint can be studied by a constrained-motion experiment. The second type of applications occurs when the robot arms are moving freely, and the only torque required at each joint is to compensate for gravity, friction and link acceleration. This problem can be simulated through a free-motion case, especially where the gear ratio is large enough for the motor inertia to dominate. In the free-motion case the amount of torque required at each joint is very low but at much higher velocities. In this paper the robust torque control of a joint for both constrained-motion, and free-motion application will be addressed in detail.

In this paper a general framework to design torque controllers for harmonic drive system is developed and tested for constrained-motion and free-motion experiments. It is shown that an empirical linear model obtained from experimental frequency responses of the system, and an uncertainty characterization of this model is sufficient to build a robust torque controller. An $\mathcal{H}_\infty$ -framework is used for controller design, and the proposed controller is tested for two different setups The closed-loop performance in time and frequency domains are shown to be exceptionally well.

II. EXPERIMENTAL SETUP

Two harmonic drive testing stations were used to monitor the behavior of two different harmonic drives, in which the harmonic drive is driven by a DC motor, and a load inertia is used to simulate the robot arm for unrestrained motion. Also a positive locking system is designed such that the output load can be locked to the ground for restrained motion experiments. In the first setup, a brushed DC motor from Electro-Craft, with maximum rated torque of 0.15 Nm, and torque constant of 0.0543 Nm/amp. The servo amplifier is an 100 Watts Electro-Craft power amplifier. The harmonic drive in this setup is from RHS series of HD systems, with gear ratio of 100:1, and rated torque of 40 Nm. In the second setup the DC motor is a brushless Kollmorgen Inland motor, with maximum rated torque of 5.6 Nm, and torque constant of 0.1815 Nm/amp. The servo amplifier is a 100 watts FAST Drive Kollmorgen. The harmonic drive is from CFS series of HD Systems, Inc. with gear ratio 160:1, and rated peak torque of 178 Nm.

Each setup is equipped with a tachometer to measure the motor velocity, and an encoder on the load side to measure the output position. The output torque is measured by a Wheatstone bridge of strain gauges mounted directly on

0-7803-4104-X/98/$10.00 ©1998 IEEE

the flexspline [8]. The current applied to the DC motor is measured from the servo amplifier output. These signals were processed by several data acquisition boards and monitored by a C-30 Challenger processor executing compiled computer C codes. Moreover, Siglab [5], a DSP hardware linked to Matlab, is used for frequency response analysis.

III. System Model and its Uncertainty

A complete model of the system was derived in [6]. To capture the system dynamics accurately, it is necessary to consider nonlinear models for friction and structural damping. However, for the purpose of control, a linear model for the system will be used for the synthesis. An empirical method to find this nominal model is to perform a series of experimental frequency response on the system, with different input amplitudes, and to find the best fit through them. By this method, not only the empirical nominal model of the system (without need of any linearization) will be determined, but also variations in the frequency response of system, due to the nonlinearities, will be encapsulated with an uncertainty representation. Using Siglab–generated sine–sweep and random inputs with different amplitudes on each experimental setup, a set of frequency response estimates for the system is generated. Applying an iterative Gauss-Newton routine on one of the frequency response estimates, a transfer function is obtained which minimizes the weighted least–squares error between the experimental frequency response and the model [1]. We call this transfer function the "Nominal Model" of the system (illustrated in Figures 1 and 2). Moreover, the variation of each frequency response estimate from the nominal model can be encapsulated by a multiplicative uncertainty. Assuming that the nominal plant transfer function is $\mathbf{P}_0(s)$, define $\mathcal{P}$ as the family of possible models of the system which includes all the experimental frequency response estimates, and the nominal model of the system, by multiplicative uncertainty we consider:

$$\forall\, \mathbf{P}(s) \in \mathcal{P}, \quad \mathbf{P}(s) = (\mathbf{1} + \mathbf{\Delta}(s)\mathbf{W}(s))\mathbf{P}_0(s) \qquad (1)$$

Here $\mathbf{W}(s)$ is a fixed transfer function, called the *uncertainty weighting function* and $\mathbf{\Delta}$ is a memoryless operator of induced norm less than unity [4]. Note that in this representation $\mathbf{\Delta}(s)\mathbf{W}(s)$ gives the normalized system variation away from 1 at each frequency:

$$\frac{\mathbf{P}(j\omega)}{\mathbf{P}_0(j\omega)} - 1 = \mathbf{\Delta}(j\omega)\mathbf{W}(j\omega) \qquad (2)$$

Hence, since $\|\mathbf{\Delta}\|_\infty \leq 1$, then

$$\left| \frac{\mathbf{P}(j\omega)}{\mathbf{P}_0(j\omega)} - 1 \right| \leq |\mathbf{W}(j\omega)|, \qquad \forall\omega \qquad (3)$$

Note that by this method an effective way to find the closest linear model for a nonlinear system is proposed, and the deviation of the nonlinear system and linear model is encapsulated in model uncertainty. For harmonic drive system the uncertainty measure at low frequencies, (as illustrated in Figures 1 and 2), is relatively small and about -5 db, which suggest the possibility of robustly controlling the system to perform within this bandwidth.

[1] Function *invfreqs* in Matlab

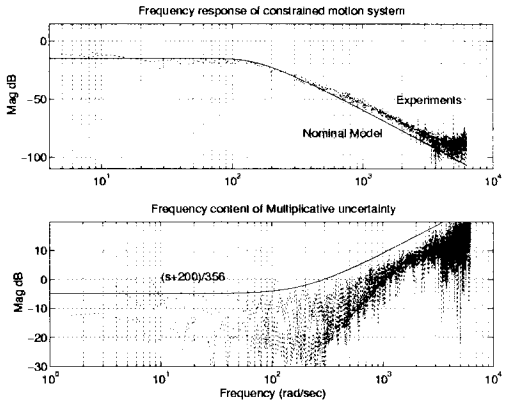

Fig. 1. Frequency response of the system under constrained–motion, nominal model, and multiplicative uncertainty

A. System under Constrained–Motion

The methodology elaborated in § III is applied for two setups to obtain their nominal model and uncertainty. Since the results are similar, here we report only the results of the first experimental setup, while the details of the other can be found in [7]. Figure 1 illustrates the empirical frequency responses of the first setup under constrained–motion, its nominal model and its uncertainty. The nominal model for the first setup is found to be a good fit to a third order stable and minimum phase transfer function as follows:

$$\frac{\text{Torque}}{\text{Ref Voltage}} = \frac{1.0755 \times 10^6}{s^3 + 472.7s^2 + 7.33 \times 10^4 s + 5.89 \times 10^6} \qquad (4)$$

which has three stable poles at -289.83, and $-91.44 \pm 109.48j$ and a DC–gain of -14.8 dB. Using Equation 3 the system variations for four typical frequency response estimates is illustrated in Figure 1, and the uncertainty weighting function is approximated by $\mathbf{W}(s) = (s + 200)/356$.

B. System under Free–Motion

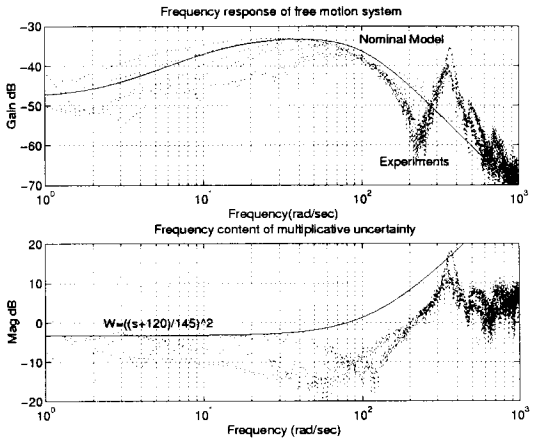

Fig. 2. Frequency response of the free–motion system, nominal model, and multiplicative uncertainty

Similar to the constrained–motion case, an empirical nominal model for the system is derived using experimental frequency response on the system for free–motion experiments. Figure 2 illustrates the empirical frequency responses of the system under free–motion, its nominal model and its uncertainty bound. The nominal model for the system is found to be a third order stable and minimum phase transfer function as follows:

$$\frac{\text{Torque}}{\text{Ref Voltage}} = \frac{243.16\ (s+2.415)}{s^3+171.19s^2+1.24\times10^4 s+1.47\times10^5} \quad (5)$$

which has three stable poles at -14.465, and $-78.363 \pm 63.288j$, and a DC–gain of -48 dB. The uncertainty weighting function is approximated by a second order system as: $\mathbf{W}(s) = \left(\frac{s+120}{145}\right)^2$. Note that the lower DC–gain in free–motion system is due to smaller torque outputs in free–motion experiments compared to the constrained–motion case. Also the system variations in free–motion are larger than that in the constrained–motion, since the nonlinear friction plays more important role for low–frequency free–motion experiments. These two factors make the control of free–motion case harder than that in the constrained–motion case.

IV. Robust Torque Control

Figure 3 illustrates the block diagram of the setup using multiplicative uncertainty representation, in which $\mathbf{P_0}$ is the nominal model of the system, $\mathbf{W}$ is the uncertainty weighting function, $\mathbf{\Delta}$ is a memoryless operator of induced norm less than unity, which represents the normalized variation of the true system from the model, and $\mathbf{C}$ is the controller. The control objective can be defined as *robustly stabilizing the system, while maintaining good disturbance attenuation and small tracking error, despite the actuator saturation.* More specifically, referring to Figure 3, we would like to design a controller to trade-off minimizing the norm of the transfer function from reference input y_d to the tracking error e (tracking performance), the transfer function from the disturbance d to the output y (disturbance attenuation), the transfer function from r to q (robust stability), and the transfer function from reference input y_d to the plant input u (actuator limit). This objective is well–suited to the general $\mathcal{H}_\infty$ problem.

Figure 4 illustrates the block diagram of the system configured for the $\mathcal{H}_\infty$ framework. It can be shown that tracking and disturbance attenuation objectives can be expressed as sensitivity $\mathbf{S}$ minimization [2]. For multiplicative uncertainty robust stability is guaranteed if the complementary sensitivity $\mathbf{T}$ has a norm less than unity (Small Gain Theorem [9]). $\mathbf{T}$ can be shown to be the transfer

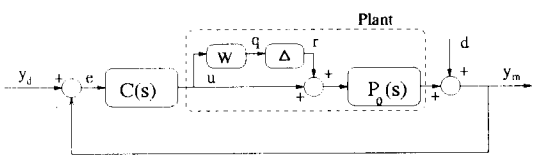

Fig. 3. Block diagram of the system considering multiplicative uncertainty for plant

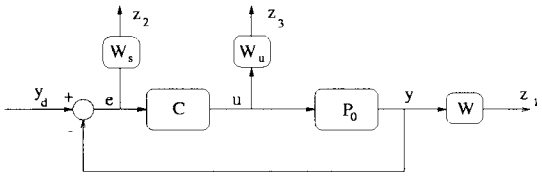

Fig. 4. Block diagram of system in $\mathcal{H}_\infty$ framework

function from reference input y_d to the output y. Weighting functions $\mathbf{W}_s$ and $\mathbf{W}_u$ are also considered to normalize and assign frequency content of the performance objectives on sensitivity and motor current saturation respectively, and $\mathbf{W}$ is the multiplicative uncertainty weighting function. Now the augmented system has one input y_d, and three outputs z_1, z_2, and z_3, in which the transfer function from the input to the outputs corresponds to weighted complementary sensitivity, weighted sensitivity, and weighted actuator effort, respectively. The objectives now will be reduced to finding the controller $C(s)$ which minimizes the induced norm of the transfer matrix from input y_d to the output vector $\mathbf{z}$ or,

$$\text{Find } C(s) \text{ to minimize } \|\mathbf{T}_{y_d\mathbf{z}}\|_\infty \quad (6)$$

This problem is called a mixed–sensitivity problem in the literature, and has optimal and sub–optimal solution algorithms. Doyle et al. [3], provided the sub–optimal solution for this problem in 1989, in which $C(s)$ will be assigned such that $\|\mathbf{T}_{y_d\mathbf{z}}\|_\infty < 1$. The μ-synthesis toolbox of Matlab uses this algorithm iteratively to find the best sub–optimal solution achievable [1].

Performance–weighting functions are selected considering the physical limitations of the system. The actuator saturation–weighting function is considered to be a constant, by which the maximum expected input amplitude never saturates the actuator. Its value is estimated to be 0.004 for the system under constrained–motion, and 0.002 for free–motion case.

The sensitivity weighting function for constrained–motion setup is assigned to be $\mathbf{W}_s(s) = \frac{s+300}{2(s+3)}$. This weighting function indicates that at low frequencies, the closed–loop system should reject disturbance at the output

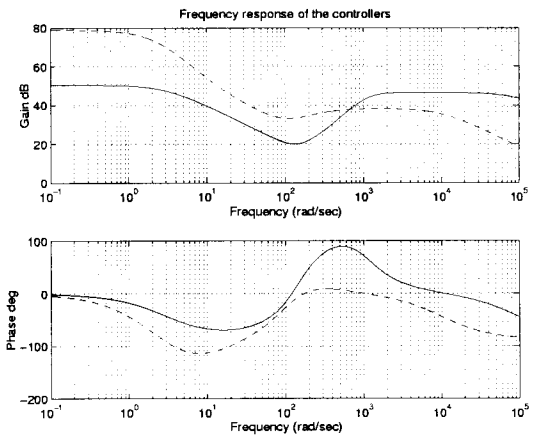

Fig. 5. The frequency response of the two designed controllers; Solid : Constrained–motion, Dashed : Free–motion

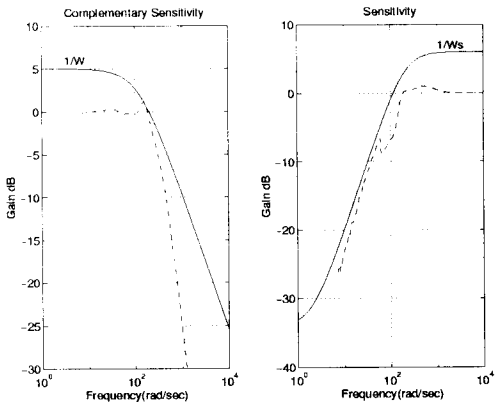

Fig. 6. Closed–loop frequency performance of the system under constrained–motion

by a factor of 50 to 1. Expressed differently steady-state tracking errors due to step input should be less than 2 % or less. This performance requirement becomes less and less stringent at higher frequencies. For higher frequencies the closed–loop frequency response should degrade gracefully, always lying underneath the inverse of the weighting function $\mathbf{W}_s$. For free–motion the sensitivity weighting function is assigned to be $\mathbf{W}_s(s) = \frac{s+280}{5(s+2.8)}$, where 5 % steady state tracking error for the closed loop system are allowed for free–motion case. The different choice of sensitivity weighting function for free–motion and constrained–motion permit us to have similar bandwith characteristics for the closed loop systems despite the lower torque output and signal to noise ratio observed in the free–motion case. For both cases the best cut-off frequency for performance is maximized by an iterative method, provided the $\mathcal{H}_\infty$ solution to the problem exist.

Two controllers were designed using μ–synthesis toolbox of Matlab. For constrained–motion case the transfer function is :

$$\mathbf{C}(s) = \frac{2.08 \times 10^7 (s + 289.8)(s + 91.4 \pm 109.5j)}{(s+3)(s + 808.2 \pm 776.04j)(s + 9.8 \times 10^4)} \quad (7)$$

with a DC–gain of 50.4 dB, while for free–motion case the controller is as follows with a DC–gain of 78.8 dB.

$$\mathbf{C}(s) = \frac{8.35 \times 10^5 (s + 14.5)(s + 78.4 \pm 63.3j)}{(s + 1.83)(s + 2.8)(s + 273.23)(s + 10^4)} \quad (8)$$

The controller zeros cancel the stable poles of the nominal plant, while the poles shape the closed–loop sensitivity function to lie underneath $\mathbf{W}_s$. Figure 5 illustrates the Bode plot of the two controllers, where for both controllers there is a wide anti-resonance profile around resonance frequency, to shape the complementary sensitivity function as flat as possible. Hence, it is not possible to obtain similar performance through a PID, or lead-lag controller.

V. Closed–Loop Performance

To verify the controller performance closed–loop experiments have been utilized. To implement the controllers in practice, bilinear discretization is performed with one kHz

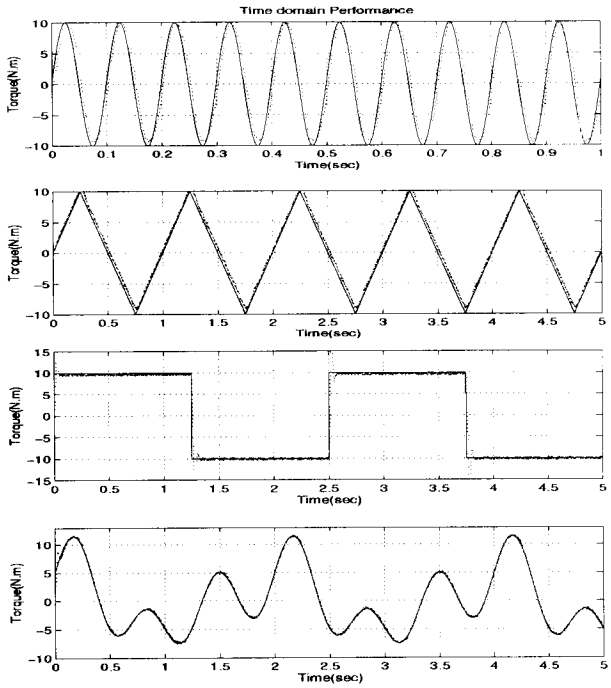

Fig. 7. Closed–loop performance of the system under constrained–motion

sampling frequency. The performance of the closed–loop system under constrained–motion and free–motion is evaluated in both frequency and time domain for two setups. However, because of the similarity in results, here only the experimental results of the first setup is presented.

A. System under Constrained–Motion

The frequency domain performance of the closed–loop system is obtained from the closed–loop frequency response of the system and is illustrated in Figure 6. For both setups the experimental sensitivity and complementary sensitivity functions are shown to be underneath the inverse of $\mathbf{W}_s$, and $\mathbf{W}$ respectively. Also the Nyquist plot for the loop-gain of the system is derived from the experimental sensitivity functions, and the phase margin is found to be 60^o. These results are an experimental verification of the $\mathcal{H}_\infty$ design claim to preserve robust stability while shaping the performance as desired.

The time response of the closed–loop system to different reference input signals is illustrated in Figure 7. The dotted lines are the measured output torque of the system, which is tracking the solid line, the reference command, very fast and accurately. Although our designed bandwidth is 3 rad/sec, sinusoid inputs up to 10 Hz (62 *rad/sec*) are shown to be well tracked. The step response is very fast with a steady–state error less than 2 % as required. Tracking of the system to triangular signal is especially sharp at the edges, and the tracking to an arbitrary signal is shown to be very fast and well-behaved.

B. System under Free–Motion

The frequency domain performance of the closed–loop system is obtained from the closed–loop frequency response

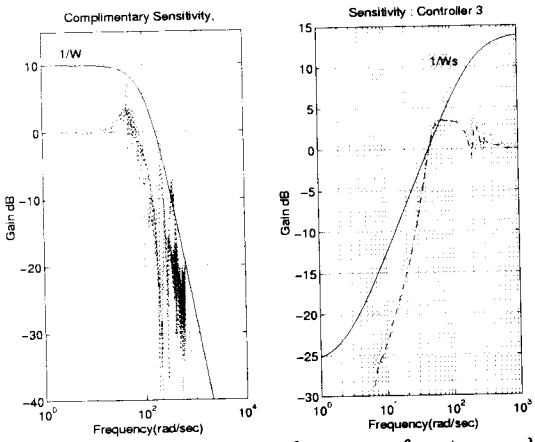

Fig. 8. Closed–loop frequency performance of system under free–motion

of the system and is illustrated in Figure 8. The experimental sensitivity and complementary sensitivity functions are shown to be underneath the inverse of $\mathbf{W}_s$, and $\mathbf{W}$ respectively. Also the Nyquist plot for the loop-gain of the system is derived from the experimental sensitivity functions, and the phase margin is found to be 80^o.

The time response of the closed–loop system to different reference input signals is illustrated in Figure 9. The dotted lines are the measured output torque of the system, which is tracking the solid line, the reference command. Although our designed bandwidth is about 2.8 rad/sec, sinusoid inputs up to 10 Hz (62 *rad/sec*) are shown to be relatively well tracked. The step response is very fast and tracking of the system to triangular signal is especially sharp at the edges. Finally, tracking to an arbitrary signal is shown to be very fast and well-behaved.

The performance of the closed–loop system under free–motion case are not as good as that in constrained–motion, because in constrained–motion experiments the open–loop system has higher DC–gain and lower uncertainty at low frequencies. Hence, wider bandwidth and better closed–loop performance are achievable as illustrated in Figure 7.

VI. Conclusions

In this paper the torque control of harmonic drive systems under constrained–motion and free–motion is examined in detail. It is illustrated how effectively an empirical nominal model for the system can be obtained through experimental frequency response estimates, and there is no need to resort to the nonlinear model of the system [6], which proved to be quite difficult to obtain. By this means not only can a linear model be proposed for the nominal model of the system, but also the deviation of the nonlinear system from the nominal model can be encapsulated in a model uncertainty. This representation provides enough information to build a robust torque controller for the harmonic drive system. It is shown that a second– or third–order transfer function can be used as a linear model of the system, and a first– order or second–order weighting function can encapsulate the multiplicative uncertainty of the model. Solving the mixed–sensitivity problem for a track-

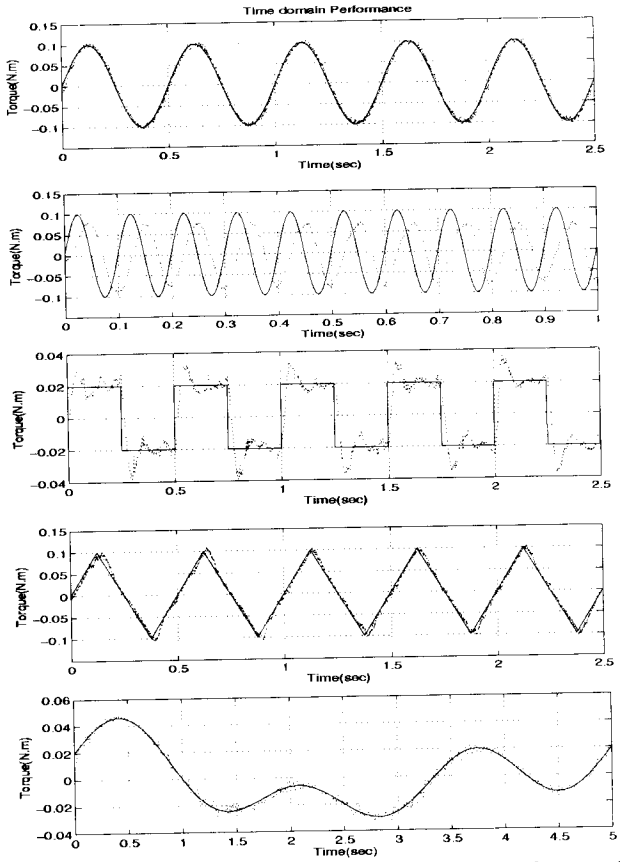

Fig. 9. Closed–loop performance of the system under free–motion

ing and disturbance attenuation objective for each case, a fourth– or fifth–order $\mathcal{H}_\infty$ controller is designed considering the actuator saturation limits. Implementing the controllers for two different setups under two different operating conditions, the performance of the closed–loop system is evaluated experimentally. It is shown that the closed–loop system retains robust stability, while improving the tracking performance exceptionally well.

References

[1] G.J. Balas, J.C. Doyle, K. Glover, A. Packard, and R. Smith. *μ–Analysis and Synthesis Toolbox*. The MathWorks, Inc., P.O. Box 1337, Minneapolis, MN 55414-5377, 1991.

[2] P.R. Bélanger. *Control engineering, a modern approach, chapter 8*. Saunders College Publishing, 6277 Sea Harbor Drive, Orlando, Florida 32887-6777, 1995.

[3] J. Doyle, K. Glover, P.P. Khargonekar, and B. A. Francis. State-space solution to standard $\mathcal{H}_2$ and $\mathcal{H}_\infty$ control problems. *IEEE Transactions on Automatic Control*, AC-34(8):831–847, 1989.

[4] J.C. Doyle, B.A. Francis, and A.R. Tannenbaum. *Feedback control theory*. Macmillan, N.Y., 1990.

[5] Signal Analysis Group. *Siglab Version 1.0*. DSP Technology Inc., 48500 Kato Road, Fremont, CA, 1994.

[6] H.D. Taghirad and P.R. Bélanger. An experimental study on modelling and identification of harmonic drive systems. *Proc. of IEEE Conf. on Decision and Control*, 4:4725–30, Dec 1996.

[7] H.D. Taghirad and P.R. Bélanger. Robust torque control of harmonic drive under constrained motion. *Proceeding of IEEE Int. Conf. on Robotics and Automation*, 1:248–253, April 1997.

[8] H.D. Taghirad, A. Helmy, and P.R. Bélanger. Intelligent built-in torque sensor for harmonic drive system. *Proceedings of the IEEE Inst. and Meas. Technology Conf.*, 1:969–974, May 1997.

[9] G. Zames. On the input-output stability of time-varying nonlinear feedback systems. *IEEE Transcript on Automatic Control*, II:228–238 (part I), and 465–476 (Part II), 1966.